Results in Chemistry 4 (2022) 100517

Contents lists available at ScienceDirect

Results in Chemistry

journal homepage: www.sciencedirect.com/journal/results-in-chemistry

Redox behaviour of imino-β-diketonato ligands and their rhodium (I) complexes

Hendrik Ferreira [a], Marrigje Marianne Conradie [a,*], Jeanet Conradie [a,b,*]

[a] Department of Chemistry, University of the Free State, P.O. Box 339, Bloemfontein 9300, South Africa
[b] Department of Chemistry, UiT - The Arctic University of Norway, N-9037 Tromsø, Norway

ARTICLE INFO

Keywords:
N,O-bidentate ligand
Redox
Rhodium
DFT
Reactivity

ABSTRACT

The redox behaviour of bidentate (BID) ligands containing either two O donor atoms (O,O'-BID ligand), a N and an O donor atom (N,O-BID ligand) or two N donor atoms (N,N'-BID ligand), and their rhodium complexes, are presented. The experimental reduction potential of the L,L'-BID ligands (L,L' = N and O) and the experimental oxidation potential of [Rh(L,L'-BID)(CO)(PPh_3)] complexes relate linearly. Though, complexes with an aromatic substituent group on the L,L'-BID ligand deviate slightly from the trend, due to the resonance effect through the extended π-system of the latter complexes. The experimental reduction potential of the L,L'-BID ligands relate linearly to the computational chemistry calculated energies of their lowest unoccupied molecular orbitals (LUMOs), whereas the experimental oxidation potential of the [Rh(L,L'-BID)(CO)(PPh_3)] complexes related linearly to the computational chemistry calculated energies of their highest occupied molecular orbitals (HOMOs). In the latter relationship it is found that the data points cluster in four groups depending on both the donor atoms (N and O) and the substituent groups (amount of CF_3 groups) on the coordinating L,L'-BID ligand.

Introduction

Bidentate (BID) ligands and their coordination compounds with d-block metals have application in many fields, such as catalysis [1], metal extraction [2], energy capture (DSSC) [3,4], energy storage (batteries) [5] and biological [6] and medial [7–9] applications. The activity of metal-BID compounds in different applications is often related to their redox activity and depends on the nature of both the metal and the ligands attached to it. The activity of the ligands is determined by the properties of their donor atoms and the substituent groups. The influence of different substituent groups on the redox activity of a series of β-diketones [10,11] and their metal complexes [12–14], as well as some imino-β-diketones [15] and their ruthenium complexes [16], are known. The β-diketonato ligand is a bidentate (BID) ligand that binds through two O donor atoms (O,O'-BID ligand) to the metal. Imino-β-diketones are similar to β-diketones, though the donor atoms are N and O, referred to as an N,O-BID ligand.

In this study the influence of different donor atoms on the redox activity of the BID-ligand and their rhodium complexes are presented. To this end we thus present an electrochemical study and computational chemistry on the N,O-BID and N,N'-BID ligands and their rhodium complexes, shown in Scheme 1. The computational chemistry study is extended to include a large range of O,O'-BID [10,11] and N,O-BID [15] ligands and rhodium-O,O'-BID complexes [17–20], to find relationships between the experimental redox potentials and computational chemistry calculated energies of the molecules.

Experimental

General

Liquid-state ^{1}H NMR spectra were recorded at 25.0 °C on a 300 MHz Bruker Avance DPX spectrometer using deuterated chloroform as solvent. The chemical shifts (δ) are reported in parts per million (ppm) and the spectra were referenced relative to Me_4Si internal standard at 0 ppm. Coupling constants (*J*) are reported in Hz. Fourier transform infrared (FTIR) measurements (solid samples) were determined with a Bruker Tensor 27 FTIR infrared spectrophotometer fitted with a Pike MIRacle single bounce and a diamond ATR, running OPUS software (Version 1.1). Reagents were obtained from Sigma-Aldrich. Solid reagents employed in preparations were used directly without further purification. Solvents were distilled prior to use. Di-μ-chloro-

* Corresponding authors.
E-mail addresses: conradiemm@ufs.ac.za (M.M. Conradie), conradj@ufs.ac.za, jco005@post.uit.no (J. Conradie).

https://doi.org/10.1016/j.rechem.2022.100517
Received 7 July 2022; Accepted 8 September 2022
Available online 13 September 2022

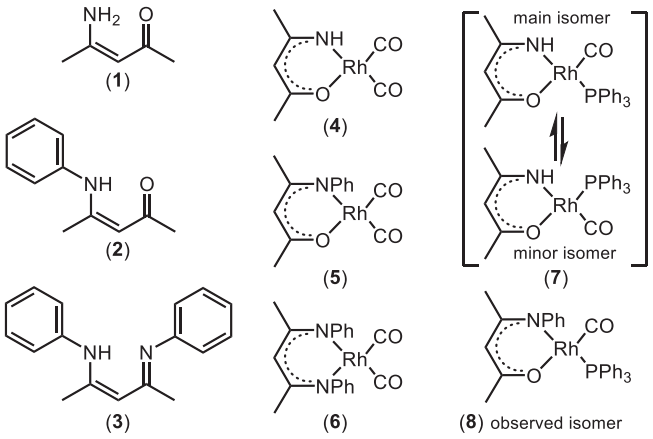

Scheme 1. Structure of ligands and complexes of this study, including complex numbers. Ph = C_6H_5 (phenyl).

tetracarbonyldirhodium(I) was obtained from Sigma-Aldrich.

Synthesis of ligands

The synthesis of the ligands was done as published in literature [21] for (**2**) and related ligands [22–26] with slight differences.

*[$CH_3COCHC(NH_2)CH_3$] **(1)***

Acetylacetone (5 g, 5.2 ml) was placed in a round bottom flask. Ammonia (6.9763 g, 7 ml) was added to the acetylacetone whilst stirring. A white solid formed. After 30 min the white solid disappeared and a yellow solution was obtained. The flask was left in a fume hood overnight. A yellow precipitate was obtained. The precipitate was filtered and dried on filter paper. Yield = 98%. Colour: yellow. M.p. 31 °C. UV: λ_{max} 291 nm, ε_{max} 12.93 $mol^{-1}dm^3cm^{-1}$ (CH_3CN). ^1H NMR: 9.723 ppm (s, N-H); 5.045 ppm (s, C-H); 2.045 ppm (s, CH_3-CN); 1.922 ppm (s, CH_3-CO).

*[$CH_3COCHC(HNPh)CH_3$] **(2)***

Acetylacetone (5 g, 5.2 ml) was placed in a round bottom flask fitted with a condenser for refluxing. Aniline (6.9763 g, 7 ml) and concentrated hydrochloric acid (5 g, 4.3 ml) was added to the flask whilst stirring and the mixture was brought to reflux for 5 hrs. Diethyl ether was added to the mixture and then placed in the fridge (-5° C). The yellow crystalline precipitate was filtered and washed with cold diethyl ether and recrystallized. Yield = 90%. Colour: light yellow. M.p. 48 °C. UV: λ_{max} 324 nm, ε_{max} 40.03 $mol^{-1}dm^3cm^{-1}$ (CH_3CN). ^1H NMR: 12.492 ppm (s, N-H); 7.388 ppm – 7.117 ppm (m, C_6H_5-N); 5.208 ppm (s, C-H); 2.122 ppm (s, CH_3-CN); 2.014 ppm (s, CH_3-CO).

*[$CH_3CNHPhCHCNPhCH_3$] **(3)***

Acetylacetone (9.75 g, 10 ml) was placed in a round bottom flask within an ice bath. Aniline (18.36 g, 18 ml) was added to the acetylacetone whilst stirring. Hydrochloric acid (9.7857 g, 8.3 ml) was added dropwise over 5 mins to the mixture and the mixture was left to stir for 5 hrs at low temperature. The mixture was then left stirring overnight. The precipitate was filtered and washed with petroleum ether, then dissolved in a mixture of dichloromethane (8 ml), water (50 ml) and triethylamine (20 ml). The solution was extracted with diethyl ether, evaporated under reduced pressure and the solid was recrystallized from ethanol. Yield = 87%. Colour: yellow. ^1H NMR: 12.720 ppm (a, N-H); 7.340 ppm – 6.972 ppm (m, 2 × C_6H_5-N); 4.906 ppm (s, C-H); 2.031 (s, 2 × CH_3-CN).

Synthesis of rhodium-dicarbonyl complexes

The synthesis and characterization of [$Rh(CH_3COCHCNHCH_3)(CO)_2$] **(4)** and [$Rh(CH_3COCHCNPhCH_3)(CO)_2$] **(5)** was done as described in literature for **(4)** [21] and **(5)** [27] and related complexes [28 29 30]. [$Rh(CH_3CN(Ph)CHCNPhCH_3)(CO)_2$] was synthesized similarly **(6).** The ligand (0.51 mmol) was dissolved in 3 ml methanol and added slowly, while stirring, to a solution of di-μ-chloro-tetracarbonyldirhodium(I) (0.10 g, 0.26 mmol) in 7 ml methanol. The mixture was left to stir for 50 min. The product was then extracted from the reaction mixture with *n*-hexane. The volume of the extracted product was reduced by slow evaporation room temperature till product precipitation. The precipitant was filtered and recrystallized.

*[$Rh(CH_3COCHCNHCH_3)(CO)_2$] **(4)***

Yield = 65%. ν_{CO}: 2044.1 cm^{-1}; 1971.0 cm^{-1}. ^1H NMR: 5.364 ppm – 5.293 ppm (d, C-H, J^4 = 2.311 Hz); 2.175 ppm – 2.172 ppm (d, CH_3-CN, J^4 = 0.74 Hz); 2.106 ppm (CH_3-CO).

*[$Rh(CH_3COCHCN(Ph)CH_3)(CO)_2$] **(5)***

Yield = 71%. ν_{CO}: 2059.0 cm^{-1}; 1997.7 cm^{-1}. ^1H NMR: 7.388 ppm – 7.061 ppm (m, C_6H_5-N); 5.298 ppm (s, C-H); 2.195 ppm (s, CH_3-CN); 2.141 ppm (s, CH_3-CO).

*[$Rh(CH_3COCN(Ph)CN(Ph)CH_3)(CO)_2$] **(6)***

Yield = 73%. ν_{CO}: 2055.6 cm^{-1}; 2046.7 cm^{-1} 1992.1 cm^{-1}; 1977.8 cm^{-1}. ^1H NMR: 7.372 ppm – 7.166 ppm (m, 2 × C_6H_5-N); 5.101 ppm (s, C-H); 1.871 ppm (s, 2 × CH_3-CN).

Synthesis of rhodium-carbonyl-phosphine complexes

The synthesis and characterization of [$Rh(CH_3COCHCNHCH_3)(CO)(PPh_3)$] **(7)** and [$Rh(CH_3COCHCNPhCH_3)(CO)(PPh_3)$] **(8)** was done as described in literature [27]. Triphenylphosphine (0.46 mmol) dissolved in 5 ml *n*-hexane, was added slowly to a solution of the 0.4 mmol rhodium-dicarbonyl complex dissolved in 5 ml *n*-hexane whilst stirring. The solution was left at room temperature till no more bubbles were evolved and product precipitation. The precipitant was filtered and recrystallized.

*[$Rh(CH_3COCHCNHCH_3)(CO)(PPh_3)$] **(7)***

Yield = 81%. ν_{CO}: 1952.7 cm^{-1}. ^1H NMR: *Isomer 1*: 7.7153 ppm – 7.352 ppm (m, C_6H_5-P); 5.101 ppm – 5.093 ppm (d, C-H, J^4 = 0.93 Hz); 2.152 ppm – 2.149 ppm (d, CH_3-CN, J^4 = 2.43 Hz); 1.676 ppm (s, CH_3-CO). *Isomer 2*: 7.715 ppm – 7.352 ppm (m, 3 × C_6H_5-P); 5.064 ppm (s, C-H); 2.062 ppm (s, CH_3-CN); 1.934 ppm (s, CH_3-CO).

*[$Rh(CH_3COCHCNPhCH_3)(CO)(PPh_3)$] **(8)***

Yield = 69%. ν_{CO}: 1966.6 cm^{-1}. ^1H NMR: 7.389 ppm – 7.061 ppm (m, C_6H_5-N; 3 × C_6H_5-P); 5.298 ppm (s, C-H); 2.142 ppm (s, CH_3-CN); 1.785 ppm (s, CH_3-CO).

Electrochemistry

Cyclic voltammetric (CV) measurements were done on a BAS100B Electrochemical Analyzer linked to a personal computer, utilizing the BAS100W Version 2.3 software. A three electrode cell setup was employed with a glassy carbon working electrode (surface area 7.07 × 10^{-6} m^2), a Pt auxiliary electrode and a Ag/Ag^+ (0.01 mol dm^{-3} $AgNO_3$ in acetonitrile) [31] reference electrode mounted on a Luggin capillary [32]. The solvent employed was anhydrous acetonitrile and the supporting electrolyte was tetra-*n*-butylammonium hexafluorophosphate ($[N(Bu_4)][PF_6]$) (0.1 mol dm^{-3}). A purified Ar gas blanket was employed and all measurements were taken at 25 °C. The concentration of the different samples was 0.001 mol dm^{-3}. Scan rates were varied between 0.05 V s^{-1} and 5.12 V s^{-1}. Repetitions with the same

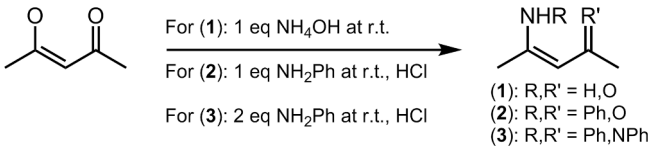

Scheme 2. Reaction pathway describing the synthesis of the desired N group containing ligands (**1**) - (**3**) from the ($CH_3COCH_2COCH_3$) starting material.

experimental conditions showed all reduction potentials were reproducible within 0.01 V. The working electrode was polished on a Bühler polishing mat, first with 1 micron and then with ¼ micron diamond paste (in a figure-of-eight motion), rinsed with EtOH, H_2O and CH_3CN, and dried before each experiment. Ferrocene was used as an internal standard and cited potentials were referenced against the Fc/Fc^+ couple, as suggested by IUPAC [33]. E_{pa} = anodic peak potential and i_{pa} = anodic peak current, E_{pc} = cathodic peak potential and i_{pc} = cathodic peak current.

DFT methods

Density functional theory (DFT) calculations were performed on the molecules using the B3LYP functional which is composed of the Becke 88 exchange functional [34] in combination with the LYP correlation functional [35], as implemented in the Gaussian 16 package [36]. The triple-ζ basis set 6-311G(d,p) was used for lighter atoms (C, H, N, F, O) and the LANL2DZ basis set that corresponds to the Los Alamos ECP plus DZ [37–39], for both the core and valence electrons of Rh. Optimizations were performed in gas phase and in CH_3CN as solvent. The implicit solvent Polarizable Continuum Model (PCM) [40] that uses the integral equation formalism variant (IEFPCM) [41] was used for solvent calculations in Gaussian. The input coordinates for the compounds were constructed using Chemcraft [42].

The population of isomers at T = 298.15 K is calculated, using the Boltzmann equation (E = electronic energy (E_{el}) or zero-point-corrected electronic energy (ZEE) or free energy (G)):

$$\ln\frac{n_j}{n_i} = -\frac{(E_j - E_i)}{kT}$$

where n_i is the number of molecules with energy E_i, and the Boltzmann's constant, $k = 1.38066 \times 10^{23}\ JK^{-1}$.

Results and discussion

Synthesis

The synthesis of the ligands was followed as published in literature [22,23]. The synthesis of the ligand (**1**), ($CH_3COCH_2CNHCH_3$), was the first reaction performed. Addition of the ammonium hydroxide solution to the ($CH_3COCH_2COCH_3$), Hacac, ligand yielded a white solid, which after a few minutes dissolved to form a yellow solution. Leaving the mixture in a fume-hood overnight allowed for the product (**1**) to crystallize out. This procedure eliminated the use of organic solvents to extract the ligand from the water solution. In this reaction between the ammonium hydroxide and the ($CH_3COCH_2COCH_3$), one of the O atoms on the ligand gets replaced by the NH group, with the remaining H atoms being consumed by the O atom to form water as by-product. The use of an acid in the reaction facilitates the formation of the water by-product. The general reaction sequence is seen in Scheme 2.

Synthesis of the ($CH_3COCH_2CNPhCH_3$), (**2**), was similar to that of (**1**), using NH_2Ph instead of NH_4OH. It was attempted to synthesize the ligand both by simple addition with low heat as well as through refluxing. The yield between the two methods (~90% for both methods) showed very little difference. The recrystallization of ligand (**2**) was slow enough to yield large crystals that had a slight off-white colour. The synthesis of ligand (**3**), ($CH_3CNPhCH_2CNPhCH_3$), was easy since the synthetic method for the synthesis of ligand (**2**) was merely left to react at a low temperature with double the amount of acid. The recrystallization of the precipitate from a slight brown coloured solution, yielded a yellow crystalline powder of high purity, as did all the synthesized ligands. The high purity was found to be evident in the NMR spectra. These spectra can be seen in Fig. 1.

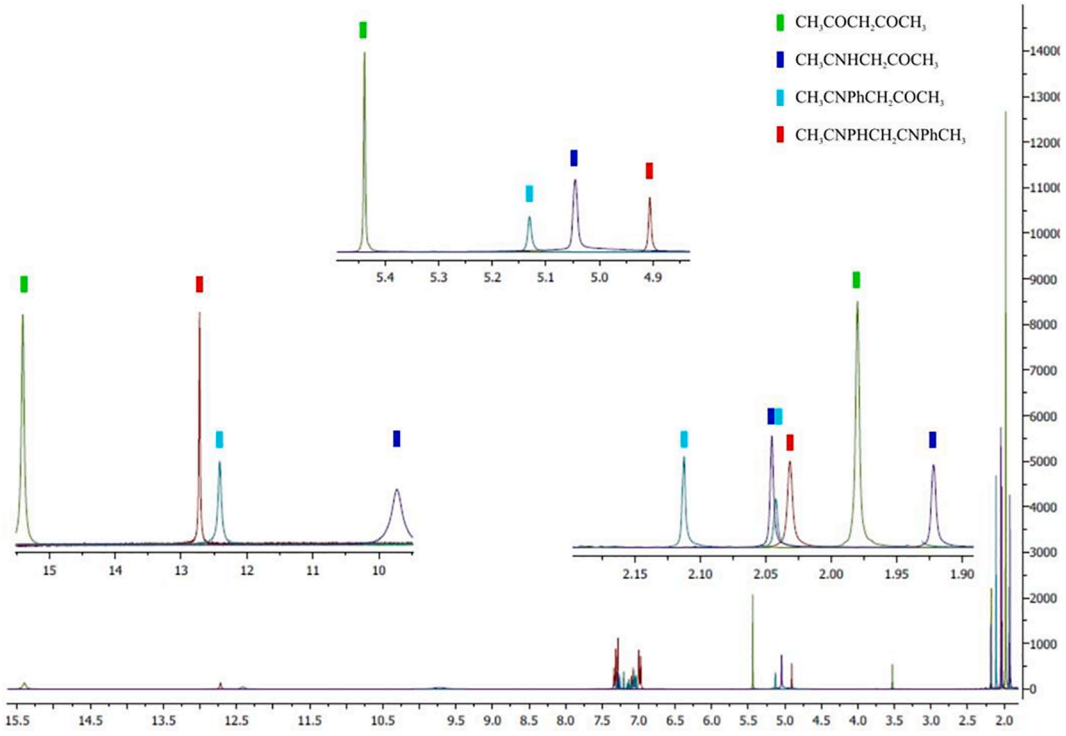

Fig. 1. Superimposed ^1H NMR spectra of all indicated ligands. X-axis show shift in ppm and y-axis relative intensity.

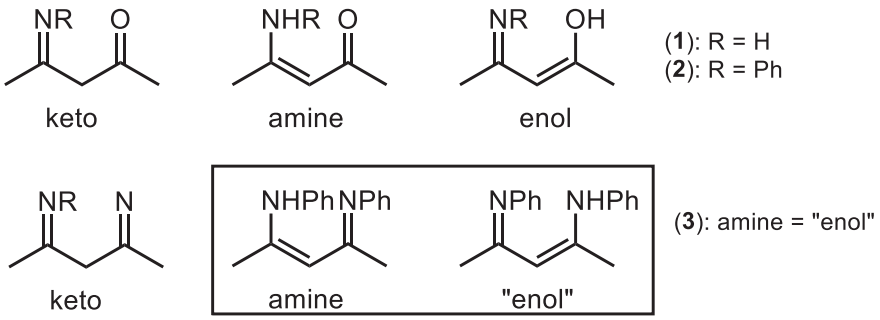

Scheme 3. Isomers possible for (1) - (3).

Table 1
Chemical shifts (σ in ppm) of the ^{1}H NMR signals for the indicated ligands in $CDCl_3$ solvent.

	Amine (N-H)	Methine (C-H)	Methyls (CH_3)	Phenyl range	Enol (O-H)
($CH_3COHCHCOCH_3$)	–	5.438 (s)	1.980 (s)	–	15.403 (s)
($CH_3COCHCNH_2CH_3$) (**1**)	9.723 (s)	5.045 (s)	2.045 (s); 1.922 (s)	–	–
($CH_3COCHCNHPhCH_3$) (**2**)	12.492 (s)	5.208 (s)	2.122 (s); 2.014 (s)	7.388–7.114 (m)	–
($CH_3CNHPhCHCNPhCH_3$) (**3**)	12.720 (s)	4.906 (s)	2.032 (s)	7.340–6.972 (m)	–

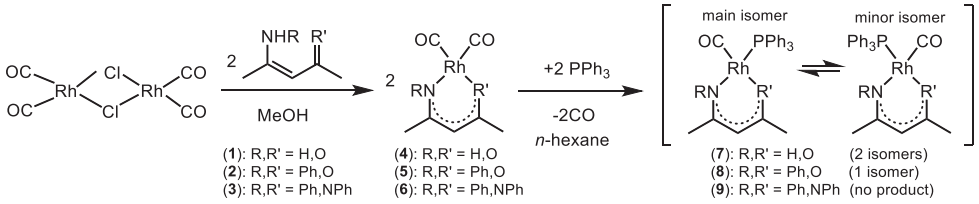

Scheme 4. Synthesis of rhodium complexes. Ph = C_6H_5 (phenyl).

For ligands (**1**) and (**2**) two possible enol and one keto isomer forms are possible. For ligand (**3**) only an "enol" and a keto isomer are possible, see Scheme 3. Since the ligands of interest in this study contain N atoms, the second possible enol form, with the H atom on the N atom, will be referred to as an amine isomer. Only a single isomeric form was observed on the NMR for (**1**) - (**3**), as illustrated in Fig. 1. This isomeric form is identified as the amine isomer, since the amine proton is observed downfield from the hydroxy proton on the NMR, see Fig. 1 and discussion below. This experimental observation also agrees with DFT calculations discussed in the DFT results section.

The NMR spectra of the ligands display no overlapping of the ^{1}H resonance peaks. The chemical shifts and the protons are summarized in Table 1 for (**1**) – (**3**). NMR shifts for ($CH_3COCH_2COCH_3$), Hacac, is added for comparative purposes. The addition of an N atom to the ligand structure causes a slight difference (Δσ = greater than 0.1 ppm) in the values of the methyl group chemical shifts of the two methyl groups. The N atom is less electronegative than the O atom ($\chi_N = 3.04$, $\chi_O = 3.44$). Therefore, there is less electron density withdrawn from the general structure towards the N atom. Thus, there is a shielding effect displayed. From Table 1 it can be seen that the effect of the more electron donating property of the substituted N atoms, relative to O, causes an upfield shift of the ^{1}H signals for the methine protons for the ($CH_3COCH_2CNPhCH_3$) (**2**), ($CH_3COCH_2CNHCH_3$) (**1**), and ($CH_3CNPhCH_2CNPhCH_3$) (**3**), ligands, and a downfield shift for the methyl protons relative to ($CH_3COCH_2COCH_3$), Hacac.

The Rh-dicarbonyl complexes (**4**) – (**6**) and the rhodium-carbonyl-

Table 2
B3LYP calculated relative electronic energies ($E)_{el}$, zero-point-corrected electronic energies (ZEE) and free energies (G), and the respective calculated population (Pop in %, using the Boltzmann equation) for the various possible isomers of the Hacac and (1) – (3), (7) and (8).

		ΔZEE (eV)	Pop (%)	ΔE_{el} (eV)	Pop (%)	ΔZEE (eV)	Pop (%)	ΔE_{el} (eV)	Pop (%)	ΔG (eV)	Pop (%)
		Solvent (CH_3CN) phase				Gas phase					
(**1**)	amine	0.00	100.00	0.00	100.00	0.00	100.00	0.00	100.00	0.00	99.92
	enol	0.31	0.00	0.39	0.00	0.31	0.00	0.30	0.00	0.31	0.00
	keto	0.54	0.00	0.54	0.00	0.54	0.00	0.55	0.00	0.18	0.08
(**2**)	amine	0.00	99.95	0.00	100.00	0.00	99.95	0.00	99.97	0.00	99.81
	enol	0.20	0.05	0.27	0.00	0.20	0.05	0.21	0.03	0.26	0.00
	keto	0.44	0.00	0.43	0.00	0.44	0.00	0.49	0.00	0.16	0.18
(**3**)	amine	0.00	100.00	0.00	100.00	0.00	100.00	0.00	100.00	0.00	99.99
	keto	0.32	0.00	0.30	0.00	0.32	0.00	0.35	0.00	0.24	0.01
Hacac	enol	0.00	99.98	0.00	99.91	0.00	99.98	0.00	99.99	0.00	99.95
	keto	0.22	0.02	0.18	0.09	0.22	0.02	0.25	0.01	0.20	0.05
(**7**)	main	0.00	99.52	0.00	97.56	0.00	99.52	0.00	99.48	0.00	99.80
	minor	0.14	0.48	0.09	2.44	0.14	0.48	0.14	0.52	0.16	0.20
(**8**)	main	0.00	100.00	0.00	100.00	0.00	100.00	0.00	100.00	0.00	100.00
	minor	0.50	0.00	0.49	0.00	0.50	0.00	0.50	0.00	0.56	0.00

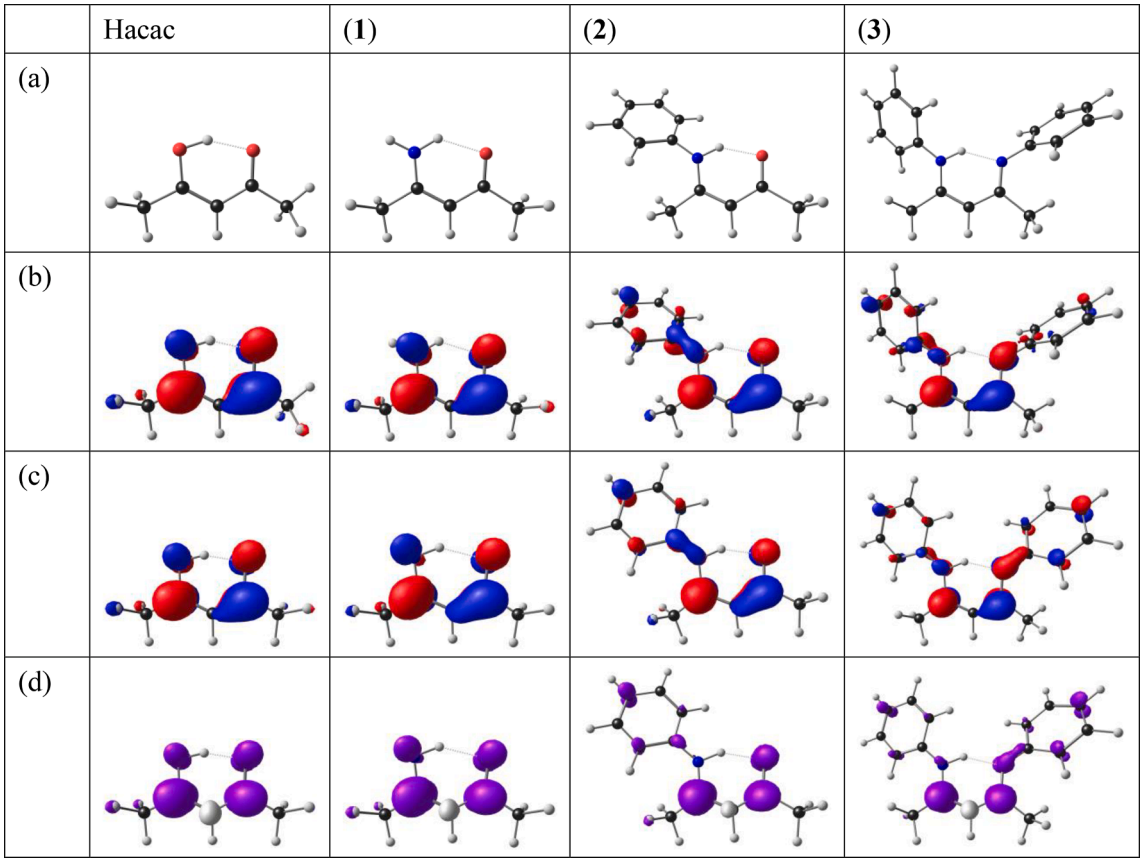

Fig. 2. B3LYP DFT calculated (a) geometry and (b) LUMO of the indicated neutral ligands, (c) HOMO and (d) spin density plots of the indicated reduced ligands. Contours of 0.06 e/Å^3 and 0.006 e/Å^3 were used for the MO and spin plots respectively. Colour code of the atoms (online version): N (blue), C (grey), O (red) and H (white). (For interpretation of the references to colour in this figure legend, the reader is referred to the web version of this article.)

phosphine complexes (**7**) and (**8**) were synthesized as described in literature [27] for (**4**), (**5**), (**7**) and (**8**). Both isomers (Scheme 4) were observed on NMR for [Rh($CH_3COCHCNHCH_3$)(CO)(PPh_3)] (**7**), while only one isomer was observed on NMR for [Rh($CH_3COCHCNPhCH_3$)(CO)(PPh_3)] (**8**). All attempts to synthesize [Rh($CH_3COCN(Ph)CN(Ph)CH_3$)(CO)(PPh_3)] from [Rh($CH_3COCN(Ph)CN(Ph)CH_3$)(CO)$_2$] (**6**) failed.

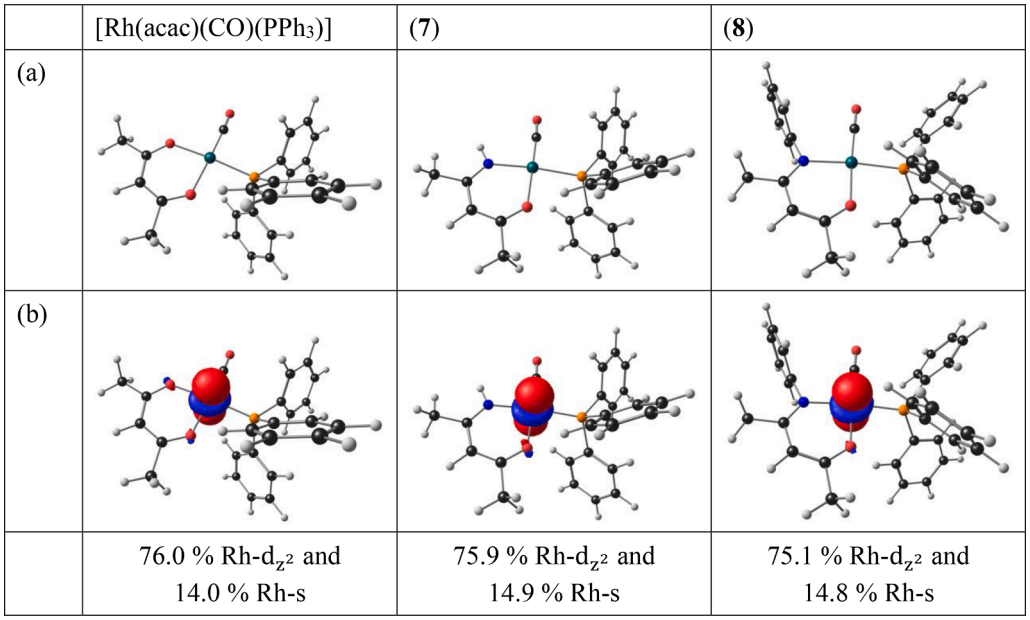

Fig. 3. B3LYP calculated (a) geometry and (b) HOMO (0.06 e/Å^3) of [Rh(acac)(CO)(PPh_3)], (**7**) and (**8**). Colour code of the atoms (online version): Rh (green), P (orange), N (blue), C (grey), O (red) and H (white). (For interpretation of the references to colour in this figure legend, the reader is referred to the web version of this article.)

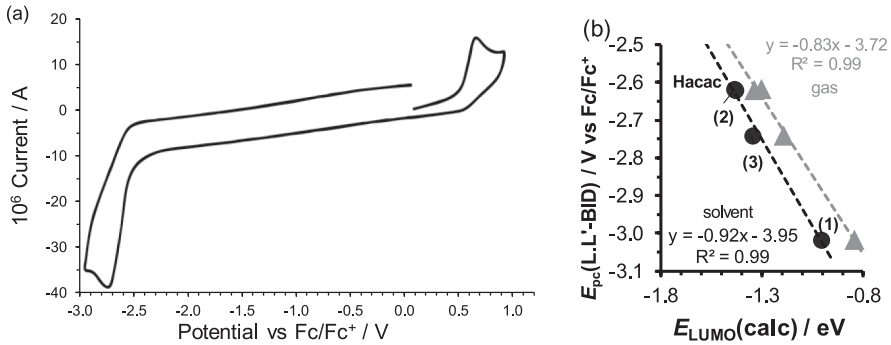

Fig. 4. (a) CV at a scan rate of 0.1 V s^{-1} of a 0.001 M acetonitrile solution containing the ($CH_3CNPhCH_2CNPhCH_3$), (**3**), and 0.1 M TBAHFP as supporting electrolyte with a glassy carbon working electrode, a Pt wire auxiliary electrode and a $Ag/AgNO_3$ reference electrode, reported *versus* Fc/Fc^+. Scans were done at room temperature, 25 °C. (b) The relationship between the reduction potentials E_{pc} of Hacac and (**1**) – (**3**) and their DFT calculated LUMO energies.

On IR and CV, it was not possible to experimentally distinguish between the different isomers of (**7**).

DFT results

Ligands (**1**) – (**3**) have one keto and one or more enol/amine isomers, see Scheme 3. The basic structure (CH_3-C(L)-C-C(L')–CH_3) of acetylacetone, Hacac, and (**1**) – (**3**) is the same - they only contain different donor atoms L and L'. Therefore, DFT results on Hacac are added for comparative reasons. The DFT calculated relative energies of the possible isomers of Hacac and (**1**) – (**3**) are given in Table 2. It is clear that for Hacac the enol and for (**1**) – (**3**) the amine isomer is the energetically favoured isomer, in agreement with experimental observation presented in the previous section.

In Fig. 2 (a) the DFT calculated optimized structures of neutral Hacac and (**1**) – (**3**) are shown. Upon reduction, an electron is added to the lowest unoccupied molecular orbital (LUMO) of the ligand, see Fig. 2 (b). This molecular orbital (MO) then becomes the highest occupied molecular orbital (HOMO) of the reduced ligand, see Fig. 2 (c). The character of the LUMO of the neutral ligand (Fig. 2 (b)) and of the HOMO of the reduced ligand (Fig. 2 (c)) is very similar. The distribution of the added electron is visualized by the spin density plot of the reduced ligand, see Fig. 2 (d), showing that the unpaired spin density in the radical anion is distributed over the *pseudo*-aromatic L-C-C-C-L' backbone (L,L' = O,O', N,O or N,N') of the ligands, extending onto the phenyl rings of the phenyl-containing ligands (**2**) and (**3**).

DFT calculations, in agreement with solid state structural data, show that the N,O-BID ligands in complexes (**7**) and (**8**) form a pseudo-aromatic six-membered ring with rhodium(I) [43–47]. In agreement with experimental observation, the DFT relative energies and calculated population in Table 2 show that complex (**7**) froms mainly (more than 97% depending on the DFT method) and complex (**8**) forms exclusively the main isomer (Scheme 1), with oxygen donor atom *trans* to the carbonyl group in the main isomer. The HOMO of these d^8 rhodium(I) complexes are mainly located on rhodium, Fig. 3, implying that electrochemical oxidation of (**7**) and (**8**), the removal of an electron(s) from the HOMO, will be rhodium based. The structure and HOMO of the structurally related Rh-O,O'-BID complex [$Rh(CH_3COCHCOCH_3)(CO)(PPh_3)$] where $CH_3COCHCOCH_3$ = acetylacetonato abbreviated as acac, are also included in Fig. 3.

CV results

The electrochemical activity of the ligands (**1**) – (**2**), using cyclic voltammetry, was reported previously. In Fig. 4 (a) a cyclic voltammogram (CV) of (**3**) over a large potential window is shown. The published peak reduction potential of the related ligand acetyl acetone ($CH_3COCH_2COCH_3$), Hacac, (**1**) and (**2**), together with the peak reduction potential of (**3**), are given in Table 3.

Table 3
Electrochemical data at a scan rate of 0.100 V $s^{-1}$of Hacac and (**1**) – (**3**), (**7**) and (**8**), from this study and from literature.

Ligands	E_{pc} *vs* Fc/Fc^+/V	Reference
($CH_3COCH_2COCH_3$)	−2.618	[11]
	−2.616	[52]
($CH_3COCH_2CNHCH_3$) (**1**)	−3.017	[15]
($CH_3COCH_2CNPhCH_3$) (**2**)	−2.617	[15]
($CH_3CNPhCH_2CNPhCH_3$) (**3**)	−2.741	this work
	E_{pa} (Rh) *vs* Fc/Fc^+/V	
[$Rh(CH_3COCHCOCH_3)(CO)(PPh_3)$]	0.357	[17]
[$Rh(CH_3CNHCHCOCH_3)(CO)(PPh_3)$] (**7**)	0.261	this work
[$Rh(CH_3COCHCNPhCH_3)(CO)(PPh_3)$] (**8**)	0.247	this work

Hacac and (**1**) – (**3**) all showed similar electrochemical behaviour, namely an irreversible reduction peak below −2.5 V *vs* Fc/Fc^+. The reduced ligand (a radical with charge −1 and spin = ½, *i.e.* containing one unpaired electron) is unstable and decomposes before it can be re-oxidised [48,10]. All the complexes displayed linearity between the peak reduction current and the square root of the scan rate, according to the Randles–Ševčík equation [11,15], indicating that the reduction of Hacac and (**1**) – (**3**) is diffusion controlled [49]. Only ($CH_3CNPhCH_2CNPhCH_3$), (**3**), displayed an oxidation that is not coupled to the observed reduction peak, at *ca* 0.7 V *vs* Fc/Fc^+, additional to the reduction peak at *ca* −2.7 V *vs* Fc/Fc^+, see Fig. 4. Both the oxidation and the reduction processes are electrochemically and chemically irreversible.

The trend of ease of reduction of the O,O-BID Hacac and the three N containing ligands (**1**) – (**3**) (Table 3), can be evaluated in terms of the different electronegativity (EN) [50] of the atoms and groups on the ligand, namely O (EN = 3.44), N (EN = 3.04), H (EN = 2.20) and Ph (EN = 2.43 [51]). The N atom is less electronegative (more electron donating) than the O atom and therefore it is expected that the three N containing ligands are reduced at lower, more negative potentials than Hacac, as indeed has been found for (**1**) and (**3**). Less electron density is withdrawn from the ligand structure towards the N atom in the neutral ligand and more energy (more negative reduction potential) is needed to add an electron to the ligand backbone of the N containing ligands. However, the Ph rings in (**2**) and (**3**) extends the conjugation through the ligand, thereby stabilizing the ligand, leading to a higher (less negative) reduction potential as expected if only the electronegativity of the O and N atoms were considered. Consequently (**2**) has the same reduction potential as Hacac. This is also in agreement with the DFT calculated similar energies of the LUMOs of Hacac and (**2**), −1.43 and −1.44 eV (gas phase) respectively and −1.34 and −1.31 eV (solvent phase calculation).

Comparing the peak cathodic potentials summarized in Table 3, of

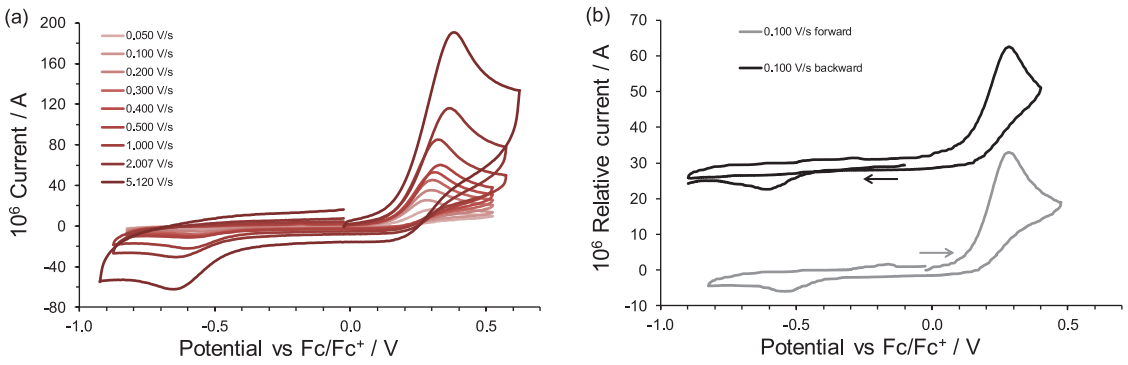

Fig. 5. (a) Cyclic voltammograms of 0.002 M [Rh($CH_3COCHCNHCH_3$)(CO)(PPh_3)] (**7**) in dry acetonitrile with 0.1 M TBAHFP as supporting electrolyte, a glassy carbon working electrode, a Pt auxiliary electrode and a Ag/$AgNO_3$ reference electrode, with scan rates ranging from 0.05 V s^{-1} to 5.12 V s^{-1}. All measurements were done at 25 °C and reported *vs* Fc/Fc^+. (b) Scans initiated first in the positive (bottom) and in the negative directions (top) of 0.002 M [Rh($CH_3COCHCNHCH_3$)(CO)(PPh_3)] (**7**) at a scan rate of 0.10 V s^{-1} and the same experimental conditions as in (a).

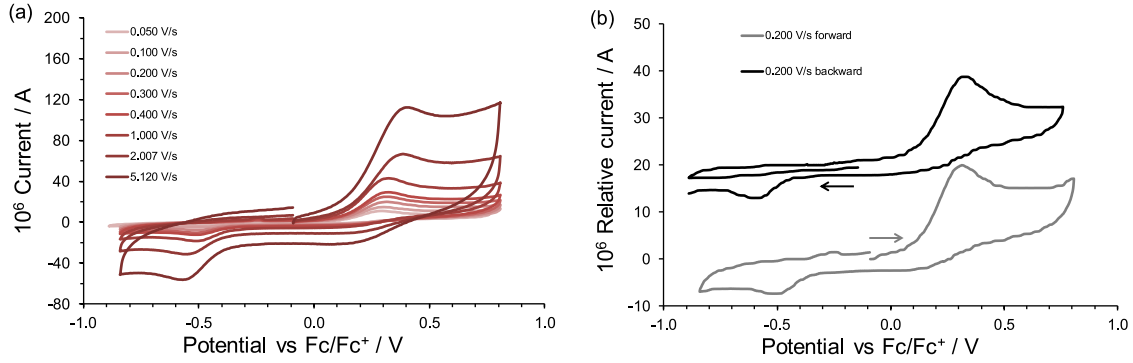

Fig. 6. (a) Cyclic voltammograms of 0.002 M [Rh($CH_3COCHCNPhCH_3$)(CO)(PPh_3)] (**8**) in dry acetonitrile with 0.1 M TBAHFP as supporting electrolyte, a glassy carbon working electrode, a Pt auxiliary electrode and a Ag/$AgNO_3$ reference electrode, with scan rates ranging from 0.05 V s^{-1} to 5.12 V s^{-1}. All measurements were done at 25 °C and reported *vs* Fc/Fc^+. (b) Scans initiated first in the positive (bottom) and in the negative directions (top) of 0.002 M [Rh($CH_3COCHCNPhCH_3$)(CO)(PPh_3)] (**8**) at a scan rate of 0.20 V s^{-1} and the same experimental conditions as in (a).

the two N,O-BID ligands (**1**) and (**2**), it can be seen that the ligand containing an H atom bonded to the N atom reduces at a more negative potential than the ligand with one Ph group bonded to the N atom. This is due to the H atom having a much smaller electronegativity than the Ph group. Less electron density is thus withdrawn from the ligand structure therefore more energy (more negative reduction potential) is needed to add an electron to ($CH_3COCH_2CNHCH_3$) (**1**). Another reason for the more positive reduction potential of the Ph containing complex (**2**) is due to the π electron density of the aromatic ring structure, stabilizing the electroactive centre of the ligand, therefore causing the more positive reduction potential.

Comparing the two Ph containing ligands, ($CH_3COCH_2CNPhCH_3$) (**2**) and ($CH_3CNPhCH_2CNPhCH_3$) (**3**), it is observed that the ($CH_3CNPhCH_2CNPhCH_3$) (**3**) ligand has a more negative reduction peak potential. The overall effect of the two N atoms on the ($CH_3CNPhCHCNPhCH_3$) (**3**) ligand *vs* the one N atom and one O atom on the ($CH_3COCHCNPhCH_3$) (**2**) ligand on the electron density of the ligands, can be compared by considering the sum of the electronegativities between the ($CH_3CNPhCH_2CNPhCH_3$) (**3**) ($EN_N + EN_N = 6$) and ($CH_3COCH_2CNPhCH_3$) (**2**) ($EN_N + EN_O = 6.5$). The ligand with smaller electronegativity, ($CH_3CNPhCH_2CNPhCH_3$) (**3**) will thus be reduced at a lower, more negative, reduction potential due to the less electron density being removed from the electroactive centre of the ligand by the less electronegative atoms in (**3**), thus increasing the amount of energy required in order to add electron density to the reduction centre. The observed order of reduction of Hacac and (**1**) – (**3**) agree with the inverted order of the order the DFT calculated energies of their LUMOs, see Fig. 4 (b).

In the electrochemical analysis of [Rh(N,O-BID)(CO)(PPh_3)] with N,O-BID = $(CH_3CNHCHCOCH_3)^-$ and $(CH_3CNPhCHCOCH_3)^-$, an oxidation peak is observed at a potential >0.2 V *vs* Fc/Fc^+, and a much smaller reduction peak more than 0.6 V away from the oxidation peak at a potential < -0.4 V *vs* Fc/Fc^+, see Fig. 5 for (**7**) and Fig. 6 for (**8**). Since oxidation of a complex involves the removal of an electron from the HOMO of the complex, that is mainly located on rhodium (Fig. 3), the first oxidation observed for (**7**) and (**8**) is assigned to the oxidation of rhodium. The electrochemical oxidation of related [Rh(β-diketonato)(CO)(PPh_3)] complexes (β-diketonato = O,O'-BID), done under the same experimental conditions, indicated a two electron oxidation of the Rh(I) to an unstable Rh(III) radical and the small reduction peak to the reduction of the evolved Rh(III) radical to an as yet unidentified Rh(I) or Rh(II) complex [9,20,53]. Both the [Rh(N,O-BID)(CO)(PPh_3)] complexes, with N,O-BID = $(CH_3CNHCHCOCH_3)^-$ (**7**) and $(CH_3CNPhCHCOCH_3)^-$ (**8**), exhibit similar structural and electronic features (Fig. 3) and showed similar experimental electrochemical behaviour to the related [Rh(β-diketonato)(CO)(PPh_3)] complexes, [20,9] therefore the oxidation and reduction peaks observed for (**7**) and (**8**) are assigned accordingly.

The [Rh($CH_3CNHCHCOCH_3$)(CO)(PPh_3)] (**7**) complex's results are used as a representative example to discuss the observed behaviour. Fig. 5 (a) contains an overlay of the CVs of (**7**) obtained at different scan rates. At slow scan rates, there is an oxidation peak present at *ca* 0.26 V *vs* Fc/Fc^+, however no reduction peak is observed in Fig. 5 (a). At higher scan rates the reduction peak appears at *ca* −0.6 V *vs* Fc/Fc^+. In order to determine the dependence of the reduction peak on the oxidation peak, the following electrochemical experiments were performed with the

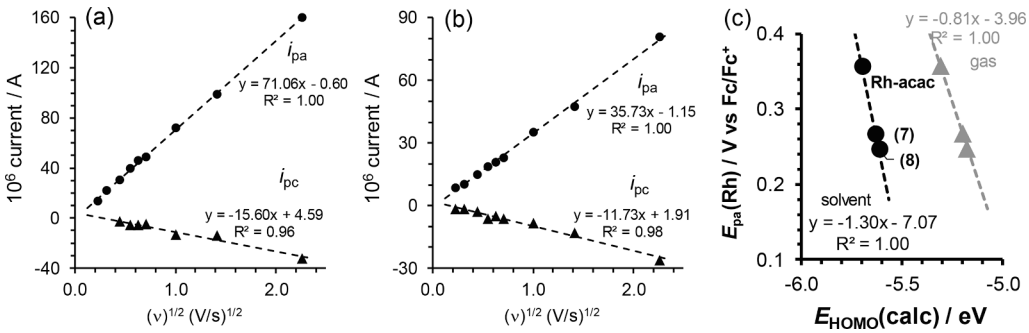

Fig. 7. Current dependence on the $\nu^{1/2}$ (ν = scan rate) for the electrochemical behaviour of (a) [Rh($CH_3COCHCNHCH_3$)(CO)(PPh_3)] (**7**) and (b) [Rh($CH_3COCHCNPhCH_3$)(CO)(PPh_3)] (**8**), in acetonitrile with a glassy carbon working electrode, $Ag/AgNO_3$ reference electrode and a Pt auxiliary electrode. The analyte concentration was 0.002 M with a 0.1 M TBAHFP supporting electrolyte. Measurements were done at 25 °C. (c) Relationship between the reduction potentials E_{pa} of [Rh($CH_3COCHCOCH_3$)(CO)(PPh_3)] and (**7**) and (**8**) and their DFT calculated HOMO energies.

results illustrated in Fig. 5 (b). The CV scans were initiated in two directions, namely one positive and one negative as seen in Fig. 5 (b). From this positive oriented scan it can be seen that the CV shows the typical curve in Fig. 5 (b) for these kind of complexes, namely an oxidation peak where the Rh(I) metal centre is oxidized and a reduction peak where the Rh(III) species is reduced. In the negative oriented scan it can be seen that as the potential is decreased, the reduction peak does not appear. After the direction is reversed and the potential is increased to a certain point, the oxidation peak occurs as per the norm. With the second direction reversal the reduction peak appears at a specific negative potential. This shows the dependence of the reduction peak on the oxidation peak. This is described as follow: In the first scan in the negative direction there are no Rh(III) species present thus there is no reduction peak. When the direction is shifted to the positive potentials the Rh(I) molecules are oxidized. Upon the second reversal there are still a sufficient amount of Rh(III) species present near the electrode surface that can be reduced and the reduction peak is observed. The same electrochemical behaviour is observed for (**8**), see Fig. 6.

The peak currents of the anodic and cathodic peaks of both (**7**) and (**8**) are far from each other (more than 0.8 V) and the reduction peak is much smaller than the oxidation peak, see Fig. 5 and Fig. 6. This shows that the redox process is electrochemically and chemically irreversible [53]. The peak oxidation and peak reduction currents are linear proportional to the square root of the scan rate as illustrated in Fig. 7. This linearity according to the Randles-Sevcik equation indicates that the oxidation and reduction processes of the Rh complexes (**7**) and (**8**) are diffusion controlled. Similar electrochemical behaviour has been observed for various [Rh(β-diketonato)(CO)(PPh_3)] complexes, where β-diketonato is an O,O'=BID ligand [17,18,54].

The oxidized Rh(III) radical generated upon oxidation, is unstable in a square planar geometry, since Rh(III) prefers an octahedral geometry. It has been proposed for related [Rh(β-diketonato)(CO)(PPh_3)] complexes on ground of experimental evidence, that the Rh(III) complex relieves the instability by the possible coordination of solvent molecules to the apical positions of the metal centre to create an octahedral geometry, thereby stabilizing the geometry [9,20]. The observed reduction peak could therefore be due to the Rh(III)-solvent adduct or another unknown Rh(III) species. Due to diffusion of the Rh(III) species that are formed during oxidation, away from the electrode surface, the observed reduction is much smaller than the oxidation. The diffusion rate may be higher than the scan rate at low scan rates and only at higher scan rates some of the Rh(III)-solvent adduct is still available near the electrode surface to be reduced back to Rh(II) or Rh(I) [9].

Distinguishing between the oxidation potential of the two possible isomers of (**7**) was not observed, even at high scan rates. This could be due to a very fast equilibrium between the two isomers, or possibly the redox potentials of the two isomers are too close together to be distinguished at this time, or that one isomer dominates in the solution.

Table 3 gives a summary of the electrochemical data obtained at 0.100 V s^{-1}, also including data of [Rh($CH_3COCHCOCH_3$)(CO)(PPh_3)]

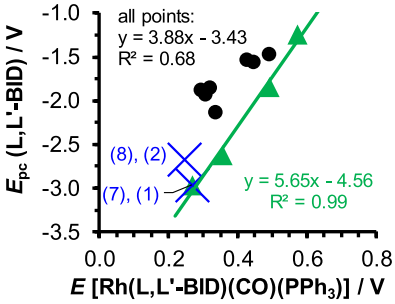

Fig. 8. The relationship between the experimental reduction potential (V *vs* Fc/Fc^+) of bidentate ligands (L,L'-BID) and the experimental oxidation potential (V *vs* Fc/Fc^+) of [Rh(L,L'-BID)(CO)(PPh_3)] complexes. The black dots indicate data of molecules containing an aromatic substituent group, the green triangles data of molecules containing no aromatic substituent groups. Data of ligands (**1**) (no aromatic substituent groups) and (2) (Ph substituent group on N) are indicated with a blue cross sign. Data in Table 4. (For interpretation of the references to colour in this figure legend, the reader is referred to the web version of this article.)

for comparative purposes. The [Rh($CH_3COCHCOCH_3$)(CO)(PPh_3)] complex with two O atoms (more electronegative than N) has the highest reduction potential, as expected. The observed order of reduction of [Rh($CH_3COCHCOCH_3$)(CO)(PPh_3)], (**6**) and (**8**) agree with the inverted order of the order the DFT calculated energies of their HOMOs, see Fig. 7 (c).

Combining CV and DFT

To a further investigation of the obtained results, redox potentials available in literature of similar bidentate ligands (L,L'-BID containing L and L' as donor atoms and substituent groups R and R' of the formula RC(L)CC(L')R' and their rhodium-carbonyl-phosphine complexes, [Rh(L,L'-BID)(CO)(PPh_3)], were evaluated, see Fig. 8. Here L,L' = O,O' or O,N or N,N'. The experimental reduction potential of the L,L'-BID ligands and the experimental oxidation potential of [Rh(L,L'-BID)(CO)(PPh_3)], shown in Fig. 8, show that data of complexes with substituent groups R and R' = CH_3 or CF_3, give a linear trend, while data of complexes with an aromatic substituent group R or R', deviate slightly from the trend. Complex (**8**) with the aromatic phenyl group on one of the N donor atoms, also deviate slightly from the trend shown in Fig. 8. It was previously found that relationships involving redox potentials of O,O'-BID ligands and metal-O,O'-BID complexes containing an aromatic substituent group on the O,O'-BID, deviate from the trend if only molecules without any aromatic substituent groups are considered [11,55], due to the resonance effect through the extended π-system.

It is, however, clear that good communication exists between L,L'-

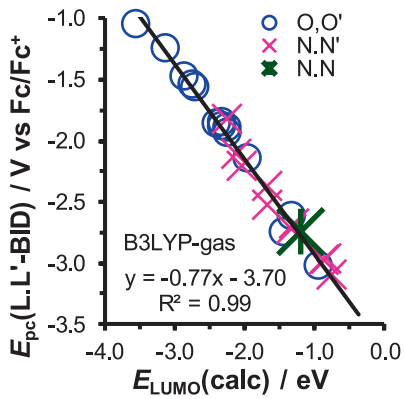

Fig. 9. The relationship between the experimental reduction potential (V *vs* Fc/Fc^+) of bidentate ligands (L,L'-BID) and the DFT calculated LUMO energy. Data in Table 4.

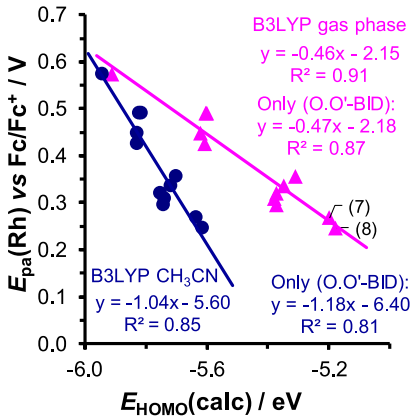

Fig. 10. The relationship between the experimental oxidation potential (V *vs* Fc/Fc^+) of [Rh(L,L'-BID)(CO)(PPh_3)] complexes and the DFT calculated HOMO energy. Data in Table 4.

BID and the metal. The oxidation potential of [Rh(L,L'-BID)(CO)(PPh_3)] is rhodium based, while the reduction of L,L'-BID occurs on the L-C-C-C-L' backbone. The implication of the trend between the experimental reduction potential of L,L'-BID and the experimental oxidation potential of [Rh(L,L'-BID)(CO)(PPh_3)], is that the reduction potential of L,L'-BID can give a good indication of the expected oxidation potential of [Rh(L,L'-BID)(CO)(PPh_3)]. Since the reactivity of [Rh(L,L'-BID)(CO)(PPh_3)] towards oxidative addition is related to the redox potential of the metal [18], the reduction potential of the L,L'-BID can give a good indication of the expected reactivity of [Rh(L,L'-BID)(CO)(PPh_3)] complexes towards oxidative addition.

The relationship between the reduction potentials of similar bidentate ligands (L,L'-BID) and their DFT calculated LUMO energies, are shown in Fig. 9. The LUMO is the MO involved in the reduction of the ligand. It is found that different β-diketones (O,O'-BID), imino-β-diketones (N,O-BID) and the di-imino-β-diketone (N,N'-BID) all lay on the same linear line of the reduction potential - LUMO energy relationship, with an accuracy level of $R^2 = 0.99$.

The relationship between the oxidation potentials of a series of [Rh(L,L'-BID)(CO)(PPh_3)] complexes and their DFT calculated HOMO energies, are shown in Fig. 10. The HOMO is the MO involved in the oxidation of the complex. In this relationship (Fig. 10) it is found that the data points cluster in four groups (also see data in Table 4):

Group 1 with N,O-BID complexes (**7**) and (**8**) of this study.
Group 2 with O,O'-BID complexes without any CF_3 substituent groups.
Group 3 with O,O'-BID complexes with one CF_3 substituent group.
Group 4 with O,O'-BID complex with two CF_3 substituent groups, [Rh(CF_3COCHCOCF_3)(CO)(PPh_3)].

It was previously found that data points involved in redox potentials relationships of the O,O'-BID-metal complexes, cluster in the three groups defined for groups 2 – 4 [56–58].

It is also observed that the linear line through groups 2 – 4 and the linear line including group 1 with the N,O-BID complexes (**7**) and (**8**) of this study, are near parallel, confirming that N,O-BID complexes indeed

Table 4
Electrochemical data (V *vs* Fc/Fc^+) and DFT calculated frontier MO energies (eV) of the indicated molecules.

L,L'-BID ligand [a]	type	L,L'-BID		[Rh(L,L'-BID)(CO)(PPh_3)]		
		E^b_{pc}	$E_{LUMO, gas}$	E_{pa} [c]	$E_{HOMO, gas}$	$E_{HOMO, CH3CN}$
CF_3COCHC(OH)(*p*-NO_2-Ph)	O,O'-BID	−1.045	−3.565			
CF_3COCHC(OH)CF_3	O,O'-BID	−1.243	−3.153	0.573	−5.912	−5.941
ThCOCHC(OH)CF_3	O,O'-BID	−1.541	−2.765	0.426	−5.606	−5.829
PhC(OH)CHCOCF_3	O,O'-BID	−1.564	−2.721	0.448	−5.620	−5.829
CH_3C(OH)CHCOCF_3	O,O'-BID	−1.851	−2.330	0.491	−5.602	−5.814
^{t}BuC(OH)CHCOCF_3	O,O'-BID	−1.889	−2.267			
ThCOCHC(OH)Th	O,O'-BID	−1.857	−2.417	0.320	−5.373	−5.751
ThCOCHC(OH)Ph	O,O'-BID	−1.884	−2.336	0.296	−5.372	−5.741
PhCOCHC(OH)Ph	O,O'-BID	−1.934	−2.256	0.308	−5.378	−5.739
CH_3COCHC(OH)CH_3	O,O'-BID	−2.618	−1.339	0.357	−5.311	−5.699
PhCOCHC(OH)CH_3	O,O'-BID	−2.138	−1.975	0.336	−5.348	−5.718
^{t}BuC(OH)CHCO^{t}Bu	O,O'-BID	−2.748	−1.446			
(CH_3O)COCHC(OH)CH_3	O,O'-BID	−3.017	−0.952			
ThThCOCHC(OH)CF_3	O,O'-BID	−1.470	−2.874	0.491	−5.601	−5.822
FuC(OH)CHCOCF_3	O,O'-BID	−1.581	−2.667			
CH_3COCHC(NH_2)CH_3	N,O-BID	−2.966	−0.844	0.268	−5.199	−5.633
CH_3COCHC(HNPh)CH_3	N,O-BID	−2.681	−1.306	0.247	−5.178	−5.614
CH_3COCHC(HN-CH_2-Ph)CH_3	N,O-BID	−2.976	−0.883			
PhCOCHC(HNPh)CH_3	N,O-BID	−2.370	−1.688			
PhCOCHC(HNPh)CF_3	N,O-BID	−1.826	−2.256			
CH_3COCHC(HN-CMe_2)CH_3	N,O-BID	−3.094	−0.762			
CH_3COCHC(HN-*p*-^{t}Bu-Ph)CH_3	N,O-BID	−2.726	−1.337			
CH_3COCHC(HN-*p*-CF_3-Ph)CH_3	N,O-BID	−2.526	−1.690			
PhCOCHC(HN-*p*-NO_2-Ph)CH_3	N,O-BID	−2.212	−2.051			
PhCOCHC(HN-3,5-Cl_2-Ph)CH_3	N,O-BID	−2.105	−2.125			
CH_3C(NPh)CHC(HNPh)CH_3	N,N'-BID	−2.741	−1.195			

a Ph = phenyl, Th = thienyl, Fu = furyl.
b Reduction potential of L,L'-BID form [10,11,15] and this study.
c Oxidation potential of [Rh(L,L'-BID)(CO)(PPh_3)] form [17–20] and this study.

follow the same trend than the O,O'-BID complexes:

E_{pa}(Rh) = -0.47 E_{HOMO}(calc gas phase)-2.15 Group 2–4
E_{pa}(Rh) = -0.46 E_{HOMO}(calc gas phase)-2.18 Group 1–4

Instead of using peak potentials in the relationships with DFT calculated frontier MOs, onset potential values [59–61] could be used. It was found for the relationship between the Cu(II/I) reduction of a series of copper(II) complexes containing 2-hydroxyphenones and the DFT calculated LUMO energies, that the relationship using peak potentials and the relationship using onset potential values, both gave linear lines with similar accuracies (R-squared values) [62].

Conclusions

Both the character of the donor groups (L and L' = N or O) and substituent groups of bidentate ligands, L,L'-BID, influence the redox chemistry of the ligands and their rhodium complexes. Aromatic substituent groups on the bidentate ligand lead to a more positive redox potential as expected due to the stabilization of the molecules through the resonance effect through the extended π-system. The electronegativity of the donor atoms and the substituent groups on the coordinating L,L'-BID ligand, leads to a clustering of the experimental oxidation potential of [Rh(L,L'-BID)(CO)(PPh_3)] complexes in four distinct groups, depending on the donor atoms and the amount of CF_3 groups on L,L'-BID.

CRediT authorship contribution statement

Hendrik Ferreira: Data curation, Formal analysis, Writing – review & editing. **Marrigje Marianne Conradie:** Conceptualization, Supervision, Resources, Validation, Methodology, Funding acquisition, Project administration, Writing – review & editing. **Jeanet Conradie:** Validation, Writing – review & editing.

Declaration of Competing Interest

The authors declare that they have no known competing financial interests or personal relationships that could have appeared to influence the work reported in this paper.

Data availability

Data will be made available on request.

Acknowledgements

This work has received support the South African National Research Foundation (grant numbers 129270 (J.C.), 132504 (J.C.) and 108960 (M.M.C.). and the Central Research Fund of the University of the Free State, Bloemfontein. The High-Performance Computing (HPC) facility of the UFS, the CHPC of South Africa (Grant No. CHEM0947) and the Norwegian Supercomputing Program (Sigma2 grant number NN9684K) are acknowledged for computer time.

Ethics Statement

This work does not require any ethical statement.

Appendix A. Supplementary data

Supplementary data to this article can be found online at https://doi.org/10.1016/j.rechem.2022.100517.

References

[1] S. Patai, The Chemistry of Metal Enolates Part 1, Wiley, 2006 www.interscience.wiley.com.
[2] J. Starý, The Solvent Extraction of Metal Chelates, Elsevier, New York, 1964, 10.1016/C2013-0-01830-0.
[3] H. Ferreira, K.G. von Eschwege, J. Conradie, Electronic properties of Fe charge transfer complexes – A combined experimental and theoretical approach, Electrochim. Acta. 216 (2016) 339–346, https://doi.org/10.1016/j.electacta.2016.09.034.
[4] J. Conradie, Polypyridyl copper complexes as dye sensitizer and redox mediator for dye-sensitized solar cells, Electrochem. Commun. 134 (2022), 107182, https://doi.org/10.1016/j.elecom.2021.107182.
[5] Q. Liu, A.A. Shinkle, Y. Li, C.W. Monroe, L.T. Thompson, A.E.S. Sleightholme, Non-aqueous chromium acetylacetonate electrolyte for redox flow batteries, Electrochem. Commun. 12 (2010) 1634–1637, https://doi.org/10.1016/j.elecom.2010.09.013.
[6] S.R. Vaidya, V.A. Shelke, S.M. Jadhav, S.G. Shankarwar, T.K. Chondhekar, Synthesis and characterization of β-diketone ligands and their antimicrobial activity, Arch. Appl. Sci. Res. 4 (2012) 1839–1843. https://www.scholarsresearchlibrary.com/abstract/synthesis-and-characterization-of–diketone-ligands-and-their-antimicrobial-activity-3186.html.
[7] B.K. Keppler, C. Friesen, H.G. Moritz, H. Vongerichten, E. Vogel, Tumor-inhibiting bis(β-Diketonato) metal complexes. Budotitane, cis-diethoxybis(1-phenylbutane-1,3-dionato)titanium(IV), in: Struct. Bond., Springer Berlin Heidelberg, Berlin, Heidelberg, 1991, pp. 97–127, 10.1007/3-540-54261-2_2.
[8] M. Gielen, E.R.T. Tiekink (Eds.), Metallotherapeutic Drugs and Metal-Based Diagnostic Agents, John Wiley & Sons Ltd, Chichester, UK, 2005, 10.1002/0470864052.
[9] J. Conradie, J.C. Swarts, The relationship between the electrochemical and chemical oxidation of ferrocene-containing carbonyl-phosphane-β-diketonato-rhodium(I) Complexes - cytotoxicity of [Rh(FcCOCHCOPh)(CO)(PPh3)], Eur. J. Inorg. Chem. 2011 (2011) 2439–2449, https://doi.org/10.1002/ejic.201100007.
[10] A. Kuhn, K.G. von Eschwege, J. Conradie, Electrochemical and density functional theory modeled reduction of enolized 1,3-diketones, Electrochim. Acta. 56 (2011) 6211–6218, https://doi.org/10.1016/j.electacta.2011.03.083.
[11] J. Conradie, N.G.S. Mateyise, M.M. Conradie, Reduction Potential of β-diketones: effect of electron donating, aromatic and ester groups, South Afr. J. Sci. Technol. 38 (2019) 1, http://www.satnt.ac.za/index.php/satnt/article/view/727.
[12] J. Conradie, Redox behaviour of [Ru(β-diketonato)3] compounds, Electrochim. Acta. 337 (2020), 135801, https://doi.org/10.1016/j.electacta.2020.135801.
[13] E. Chiyindiko, J. Conradie, Redox behaviour of bis(β-diketonato)copper(II) complexes, J. Electroanal. Chem. 837 (2019) 76–85, https://doi.org/10.1016/j.jelechem.2019.02.011.
[14] R. Gostynski, M.M. Conradie, R.Y. Liu, J. Conradie, Electronic influence of different β-diketonato ligands on the electrochemical behaviour of tris(β-Diketonato)M(III) complexes, M = Cr, Mn and Fe, J. Nano Res. 44 (2016) 252–264, https://doi.org/10.4028/www.scientific.net/JNanoR.44.252.
[15] T.L. Ngake, J.H. Potgieter, J. Conradie, Electrochemical behaviour of amino substituted β-amino α, β-unsaturated ketones: A computational chemistry and experimental study, Electrochim. Acta. 296 (2019) 1070–1082, https://doi.org/10.1016/j.electacta.2018.11.144.
[16] T.L. Ngake, J.H. Potgieter, J. Conradie, Tris(β-ketoiminato)ruthenium(III) complexes: Electrochemical and computational chemistry study, Electrochim. Acta. 320 (2019), 134635, https://doi.org/10.1016/j.electacta.2019.134635.
[17] H. Ferreira, M.M. Conradie, J. Conradie, Electrochemical study of carbonyl phosphine β-diketonato rhodium(I) complexes, Electrochim. Acta. 113 (2013) 519–526, https://doi.org/10.1016/j.electacta.2013.09.099.
[18] N.G.S. Mateyise, J. Conradie, M.M. Conradie, Synthesis, characterization, electrochemistry, DFT and kinetic study of the oligothiophene-containing complex [Rh((C4H3S-C4H2S)COCHCOCF3)(CO)(PPh3)], Polyhedron. 199 (2021), 115095, https://doi.org/10.1016/j.poly.2021.115095.
[19] J. Conradie, Density functional theory calculations of Rh-β-diketonato complexes, Dalt. Trans. 44 (2015) 1503–1515, https://doi.org/10.1039/C4DT02268H.
[20] D. Lamprecht, G.J. Lamprecht, Electrochemical oxidation of Rh(I) to Rh(III) in rhodium(I) β-diketonato carbonyl phosphine complexes, Inorg. Chim. Acta. 309 (2000) 72–76, https://doi.org/10.1016/S0020-1693(00)00235-8.
[21] H. Ferreira, M.M. Conradie, P.H. van Rooyen, J. Conradie, Packing polymorphism of dicarbonyl-[2-(phenylamino)pent-3-en-4-onato]rhodium(I), J. Organomet. Chem. 851 (2017) 235–247, https://doi.org/10.1016/j.jorganchem.2017.09.039.
[22] S.G. McGeachin, Synthesis and properties of some β-diketimines derived from acetylacetone, and their metal complexes, Can. J. Chem. 46 (1968) 1903–1912, https://doi.org/10.1139/v68-315.
[23] M. Lacey, Convenient syntheses of 4-Aminopent-3-en-2-one and its copper and nickel complexes, Aust. J. Chem. 23 (1970) 841, https://doi.org/10.1071/CH9700841.
[24] A.P. Dove, V.C. Gibson, E.L. Marshall, A.J.P. White, D.J. Williams, Magnesium and zinc complexes of a potentially tridentate β-diketiminate ligand, Dalt. Trans. (2004) 570–578, https://doi.org/10.1039/B314760F.
[25] J.E. Parks, R.H. Holm, Synthesis, solution stereochemistry, and electron delocalization properties of bis(.beta.-iminoamino)nickel(II) complexes, Inorg. Chem. 7 (1968) 1408–1416, https://doi.org/10.1021/ic50065a029.
[26] P.H.M. Budzelaar, N.N.P. Moonen, R. de Gelder, J.M.M. Smits, A.W. Gal, Rhodium and Iridium β-Diiminate Complexes – Olefin Hydrogenation Step by Step, Eur. J. Inorg. Chem. 2000 (2000) 753–769, https://doi.org/10.1002/(SICI)1099-0682(200004)2000:4<753::AID-EJIC753>3.0.CO;2-V.

[27] H. Ferreira, M.M. Conradie, J. Conradie, Kinetic study of the oxidative addition reaction between methyl iodide and [Rh(imino-β-diketonato)(CO)(PPh)3] complexes, utilizing UV–Vis, IR spectrophotometry, NMR spectroscopy and DFT calculations, Molecules 27 (2022) 1931, https://doi.org/10.3390/molecules27061931.

[28] F. Bonati, G. Wilkinson, 600. Dicarbonyl-β-diketonato- and related complexes of rhodium(I), J. Chem. Soc. (1964) 3156–3160, https://doi.org/10.1039/JR9640003156.

[29] A.I. Ruballo, V.P. Selina, T.G. Cherkasova, Y.S. Varshavskii, IR-spectroscopic study of dicarbonyl complexes of rhodium (I) with β-aminovinyl ketones by Ruballo Selina Cherkasova Varshavskii, Koord. Khimiya. 17 (1992) 530–536.

[30] M.R. Galding, T.G. Cherkasova, L.V. Osetrova, Y.S. Varshavsky, 31P NMR spectra of beta-aminovinylketonato rhodium (I) carbonyl-phosphine complexes Rh(AVK)(PPh3) (CO), Rhodium Express. 1 (1993) 14–17.

[31] D.T. Sawyer, J.J.L. Roberts, Experimental Electrochemistry for Chemists, John Wiley & Sons Ltd., 1974, 10.1002/bbpc.19750790937.

[32] P.T. Kissinger, W.R. Heineman, D.H. Evans, K.M. O'Connell, R.A. Petersen, M. J. Kelly, Cyclic voltammetry, J. Chem. Educ. 60 (1983) 702–706, https://doi.org/10.1021/ed060p702.

[33] G. Gritzner, J. Kuta, Recommendations on reporting electrode potentials in nonaqueous solvents (Recommendations 1983), Pure Appl. Chem. 56 (1984) (1983) 461–466, https://doi.org/10.1351/pac198456040461.

[34] A.D. Becke, Density-functional exchange-energy approximation with correct asymptotic behavior, Phys. Rev. A. 38 (1988) 3098–3100, https://doi.org/10.1103/PhysRevA.38.3098.

[35] C. Lee, W. Yang, R.G. Parr, Development of the Colle-Salvetti correlation-energy formula into a functional of the electron density, Phys. Rev. B. 37 (1988) 785–789, https://doi.org/10.1103/PhysRevB.37.785.

[36] M.J. Frisch, G.W. Trucks, H.B. Schlegel, G.E. Scuseria, M.A. Robb, J.R. Cheeseman, G. Scalmani, V. Barone, G.A. Petersson, H. Nakatsuji, X. Li, M. Caricato, A. V. Marenich, J. Bloino, B.G. Janesko, R. Gomperts, B. Mennucci, H.P. Hratchian, J. V. Ortiz, A.F. Izmaylov, J.L. Sonnenberg, D. Williams-Young, F. Ding, F. Lipparini, F. Egidi, J. Goings, B. Peng, A. Petrone, T. Henderson, D. Ranasinghe, V.G. Zakrzewski, J. Gao, N. Rega, G. Zheng, W. Liang, M. Hada, M. Ehara, K. Toyota, R. Fukuda, J. Hasegawa, M. Ishida, T. Nakajima, Y. Honda, O. Kitao, H. Nakai, T. Vreven, K. Throssell, J. Montgomery, J. A., J.E. Peralta, F. Ogliaro, M.J. Bearpark, J.J. Heyd, E.N. Brothers, K.N. Kudin, V.N. Staroverov, T.A. Keith, R. Kobayashi, J. Normand, K. Raghavachari, A.P. Rendell, J.C. Burant, S.S. Iyengar, J. Tomasi, M. Cossi, J.M. Millam, M. Klene, C. Adamo, R. Cammi, J.W. Ochterski, R.L. Martin, K. Morokuma, O. Farkas, J.B. Foresman, D.J. Fox, Gaussian 16, Revision B.01, (2016).

[37] P.J. Hay, W.R. Wadt, Ab initio effective core potentials for molecular calculations. Potentials for the transition metal atoms Sc to Hg, J. Chem. Phys. 82 (1985) 270–283, https://doi.org/10.1063/1.448799.

[38] W.R. Wadt, P.J. Hay, Ab initio effective core potentials for molecular calculations. Potentials for main group elements Na to Bi, J. Chem. Phys. 82 (1985) 284–298, https://doi.org/10.1063/1.448800.

[39] P.J. Hay, W.R. Wadt, Ab initio effective core potentials for molecular calculations. Potentials for K to Au including the outermost core orbitale, J. Chem. Phys. 82 (1985) 299–310, https://doi.org/10.1063/1.448975.

[40] A.V. Marenich, C.J. Cramer, D.G. Truhlar, Universal solvation model based on solute electron density and on a continuum model of the solvent defined by the bulk dielectric constant and atomic surface tensions, J. Phys. Chem. B. 113 (2009) 6378–6396, https://doi.org/10.1021/jp810292n.

[41] R.E. Skyner, J.L. Mcdonagh, C.R. Groom, T. Van Mourik, A review of methods for the calculation of solution free energies and the modelling of systems in solution, Phys. Chem. Chem. Phys. 17 (2015) 6174–6191, https://doi.org/10.1039/C5CP00288E.

[42] Chemcraft - graphical software for visualization of quantum chemistry computations., (n.d.). http://www.chemcraftprog.com/.

[43] L.J. Damoense, W. Purcell, A. Roodt, J.G. Leipoldt, The Crystal Structure of (2-Aminovinyl-4-pentanonato-KO, KN)-carbonyl-triphenylphosphinerhodium (I), Rhodium Express. 5 (1994) 10–13.

[44] G.J.S. Venter, G. Steyl, A. Roodt, Crystal structure of carbonyl-(4-(2,6-dichlorophenylamino)pent-3-en-2-onato-κ2N, O)-(triphenylphosphine-κP)-rhodium(I) acetone solvate, C31.5H28Cl2NO2.5PRh, Zeitschrift Für Krist. - New Cryst. Struct. 228 (2013) 410–412, https://doi.org/10.1524/ncrs.2013.0172.

[45] G.J.S. Venter, The crystal structure of carbonyl-[4-(2,4-dichlorophenylamino)pent-3-en-2-onato-κ2N,O]-(triphenylphosphine-κP)rhodium(I), RhC30H25Cl2NO2P, Zeitschrift Für Krist. - New Cryst. Struct. 232 (2017) 901–903, https://doi.org/10.1515/ncrs-2017-0059.

[46] G.J.S. Venter, G. Steyl, A. Roodt, Carbonyl[4-(2,3-dimethylphenylamino)pent-3-en-2-onato-κ 2 N, O](triphenylphosphine-κ P)rhodium(I), Acta Crystallogr, Sect. E Struct. Reports Online. 65 (2009) m1321–m1322, https://doi.org/10.1107/S1600536809039816.

[47] G.J.S. Venter, G. Steyl, A. Roodt, Carbonyl[4-(2,6-dimethylphenylamino)pent-3-en-2-onato-κ2 N, O](triphenylphosphine-κP)rhodium(I) acetone hemisolvate, Acta Crystallogr, Sect. E Struct. Reports Online. 65 (2009) m1606–m1607, https://doi.org/10.1107/S160053680904817X.

[48] R.C. Buchta, D.H. Evans, Mechanism of the electrochemical reduction of enolized 1,3-diketones, J. Electrochem. Soc. 117 (1970) 1494, https://doi.org/10.1149/1.2407358.

[49] D.H. Evans, K.M. O'Connell, R.A. Petersen, M.J. Kelly, Cyclic voltammetry, J. Chem. Educ. 60 (1983) 290, https://doi.org/10.1021/ed060p290.

[50] J.E. Huheey, The electronegativity of groups, J. Phys. Chem. 69 (1965) 3284–3291, https://doi.org/10.1021/j100894a011.

[51] P.R. Wells, Group electronegativities, in: A. Streitwieser, R.W. Taft (Eds.), Prog. Phys. Org. Chem., John Wiley & Sons, Inc., Hoboken, NJ, USA, 1968, pp. 111–145, doi:10.1002/9780470171851.ch3.

[52] T.E. Neal, R.W. Murray, Autocatalysis of the kinetic wave of acetylacetone in acetonitrile solvent, Anal. Chem. 42 (1970) 1654–1656, https://doi.org/10.1021/ac60295a017.

[53] J.J.C. Erasmus, J. Conradie, Chemical and electrochemical oxidation of [Rh(β-diketonato)(CO)(P(OCH2)3CCH3)]: an experimental and DFT study, Dalt. Trans. 42 (2013) 8655, https://doi.org/10.1039/c3dt50310k.

[54] N.F. Stuurman, B.E. Buitendach, L. Twigge, P.J. Swarts, J. Conradie, Rhodium (triphenylphosphine)carbonyl-2,4-dioxo-3-pentyl-4-decanyloxybenzoate: synthesis, electrochemistry and oxidative addition kinetics, New J. Chem. 42 (2018) 4121–4132, https://doi.org/10.1039/C7NJ05039A.

[55] J. Conradie, Redox chemistry of tris(β-diketonate)cobalt(III) complexes: A molecular view, J. Electrochem. Soc. 169 (2022), 046522, https://doi.org/10.1149/1945-7111/ac6705.

[56] M.M. Conradie, J. Conradie, Electrochemical behaviour of Tris(β-diketonato)iron (III) complexes: A DFT and experimental study, Electrochim. Acta. 152 (2015) 512–519, https://doi.org/10.1016/j.electacta.2014.11.128.

[57] R. Freitag, J. Conradie, Electrochemical and computational chemistry study of Mn (β-diketonato)3 complexes, Electrochim. Acta. 158 (2015) 418–426, https://doi.org/10.1016/j.electacta.2015.01.147.

[58] R. Liu, J. Conradie, Tris(β-diketonato)chromium(III) complexes: Effect of the β-diketonate ligand on the redox properties, Electrochim. Acta. 185 (2015) 288–296, https://doi.org/10.1016/j.electacta.2015.10.116.

[59] Y.H. Budnikova, Y.B. Dudkina, A.A. Kalinin, M.Y. Balakina, Considerations on electrochemical behavior of NLO chromophores: Relation of redox properties and NLO activity, Electrochim. Acta. 368 (2021), 137578, https://doi.org/10.1016/j.electacta.2020.137578.

[60] S. Pluczyk, M. Vasylieva, P. Data, Using cyclic voltammetry, UV-Vis-NIR, and EPR spectroelectrochemistry to analyze organic compounds, J. Vis. Exp. (2018) 1–13, https://doi.org/10.3791/56656.

[61] A.A. Adeniyi, T.L. Ngake, J. Conradie, Cyclic voltammetric study of 2-hydroxybenzophenone (HBP) Derivatives and the correspondent change in the orbital energy levels in different solvents, Electroanalysis. 32 (2020) 2659–2668, https://doi.org/10.1002/elan.202060163.

[62] E. Chiyindiko, E.H.G. Langner, J. Conradie, Electrochemical behaviour of copper (II) complexes containing 2-hydroxyphenones, Electrochim. Acta. 424 (2022), 140629, https://doi.org/10.1016/j.electacta.2022.140629.